JACS
JOURNAL OF THE AMERICAN CHEMICAL SOCIETY
Article
pubs.acs.org/JACS

Electron Transfer in Quantum-Dot-Sensitized ZnO Nanowires: Ultrafast Time-Resolved Absorption and Terahertz Study

Karel Žídek,[†,‡] Kaibo Zheng,[†,‡] Carlito S. Ponseca, Jr.,[†] Maria E. Messing,[§] L. Reine Wallenberg,[∥] Pavel Chábera,[†] Mohamed Abdellah,[†] Villy Sundström,[†] and Tõnu Pullerits*,[†]

[†]Department of Chemical Physics, Lund University, Box 124, 22100 Lund, Sweden
[§]Solid State Physics, Lund University, Box 118, 22100 Lund, Sweden
[∥]Center for Analysis and Synthesis/nCHREM, Lund University, Box 124, 22100 Lund, Sweden

S *Supporting Information*

ABSTRACT: Photoinduced electron injection dynamics from CdSe quantum dots to ZnO nanowires is studied by transient absorption and time-resolved terahertz spectroscopy measurements. Ultrafast electron transfer from the CdSe quantum dots to ZnO is proven to be efficient already on a picoseconds time scale (τ = 3−12 ps). The measured kinetics was found to have a two-component character, whose origin is discussed in detail. The obtained results suggest that electrons are injected into ZnO via an intermediate charge transfer state.

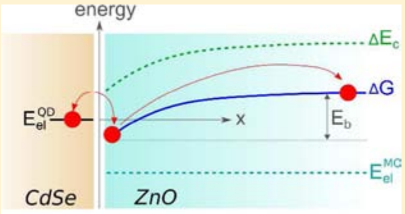

INTRODUCTION

Immense interest in photovoltaics during the last decades has resulted in number of approaches to solar cells (SCs) construction. Among various concepts, utilization of semiconductor quantum dots (QDs) attached to a metal oxide (MO) surface has attracted much attention due to several merits of QDs.[1−10] In comparison to analogous dye-sensitized SCs, QDs offer good photostability,[8] a tunable absorption edge,[11] and the possibility of multiple exciton generation and collection.[9] However, the overall performance of QD-sensitized SCs obtained to date (up to 4.9% conversion efficiency)[12] is far below the theoretically expected values (15−20%),[13] and a substantial improvement is needed for eventual applications.

The high efficiency of QD-sensitized SCs is known to be conditioned by a rapid electron transport from QD to the MO, but in spite of efforts toward understanding this process,[1−7] the results remain controversial. Reported time scales of electron transfer vary from picoseconds[2] up to nanoseconds,[14] and various interpretations of observed kinetics can be found.

Ambiguity in the reports has several reasons. For example, most of the studies use only transient absorption (TA) or photoluminescence measurements,[1−10] which are sensitive to a change in the number of excited electrons in QDs, but cannot clearly distinguish various processes leading to that change. Second, QDs with surface defects are often used for the measurements. Thus, electron surface trapping coexists with the electron transfer. This further complicates the already nontrivial kinetics and may hinder the transfer.

In this article, we overcome both the above-mentioned shortcomings. We study the process of electron transfer from the QD to the MO by employing a combination of TA measurements and time-resolved terahertz (THz) spectroscopy. The two methods are complementary for the study of the QD−MO system because TA can be used to track down the excited electrons in CdSe QDs, while THz spectroscopy is sensitive to the mobility of carriers and can thereby detect appearance of the excited electrons in the MO. Moreover, we use high-quality QDs that do not show any fast kinetics related to the surface trapping. The choice of a sample is essential, as evident from the previous attempt of Pijpers et al. to observe the electron transfer in QD-sensitized MO by THz spectroscopy.[15]

Employing ZnO as an electron acceptor brings several advantages. For example, electrons in ZnO have high mobility. This leads to efficient transport through ZnO to an electrode, and also makes it easy to detect the injected electrons in ZnO via THz spectroscopy. Furthermore, ZnO features easy crystallization with anisotropic growth producing well-organized morphologies.[16] A number of previous studies of CdSe−ZnO systems report electron transfer rates and performance of real SCs, presenting comparisons of various MOs, linker molecules, and surface chemistry.[2,17−21] However, due to the above-mentioned ambiguity of the TA method and sample properties, the studies did not lead to any consensus on the electron transfer rate in the system.

Our measurements provide a clear and direct evidence of an ultrafast electron transfer from CdSe QDs to ZnO nanowires (NWs) on a picosecond time scale. Moreover, our results suggest that the electrons excited in QDs are injected into ZnO via an intermediate charge-transfer state (CTS).

EXPERIMENTAL SECTION

Sample Preparation. Synthesis of ZnO NWs followed the widely known hydrothermal method.[16] Oleic acid capped CdSe QDs were synthesized using trioctylphosphine selenide (TOP-Se) solution as a

Received: March 27, 2012
Published: June 25, 2012

dx.doi.org/10.1021/ja3029679 | *J. Am. Chem. Soc.* 2012, 134, 12110−12117

Se^{2-} source and CdO as a Cd^{2+} source. The reaction temperature was varied from 180 to 240 °C to obtain QDs with different sizes. The capping agent on the QDs was exchanged to a bifunctional molecule containing a thiol group (2-mercaptopropionic acid) and the QDs were dissolved in polar solvent (ethanol). For sensitization, the ZnO NWs were immersed into linker-capped CdSe QDs ethanol solution in the dark. For further details see Supporting Information.

Morphology Characterization. The morphologies of CdSe QDs, ZnO NWs and CdSe QD sensitized ZnO NWs were characterized via scanning electron microscopy (SEM, LEO 1650) and high resolution analytical transmission electron microscopy (HR-TEM, JEOL 3000F equipped with Oxford SDD X-ray analyzer). The optical absorption spectra were recorded on an Agilent 845x absorption spectrophotometer.

Transient Absorption. TA measurements were carried out using a standard pump−probe setup. Laser pulses (800 nm, 80 fs pulse length, 1 kHz repetition rate) were generated by a regenerative amplifier (Spitfire) seeded by a femtosecond oscillator (Tsunami, both Spectra Physics). Excitation pulses at 470 nm were generated by an optical parametric amplifier (OPA; Topas, Light Conversion). The excitation photon flux of 8×10^{13} photons/cm^2/pulse corresponds to $N = 0.15$ (mean number of excited e-h pairs per QD). For the probe pulses we used either the supercontinuum generation from a thin sapphire plate (TA spectra measurements) or an OPA (Topas) conversion to wavelengths from 506 to 542 nm (TA kinetics measurements).

Under the excitation intensities used for TA measurements, samples undergo slight photodegradation (less than 5% in one scan).[22,23] Its cumulative effect was avoided by shifting the sample to a fresh spot after each scan.

THz Spectroscopy. The same laser system used in TA measurements was utilized for THz spectroscopy. The laser beam was split into three. The first beam generates THz radiation by optical rectification in a 1 mm thick (110) ZnTe crystal. The second beam was used in another (110) ZnTe crystal for detection of THz pulses via electro-optical sampling. The third beam seeds an OPA (Topas) generating 529-nm pulses used for sample photoexcitation with a fluence of 6.3×10^{14} photons/cm^2/pulse ($N = 1.2$). To avoid absorption of THz radiation due to water vapor and possible photodegradation of the sample, the THz apparatus was placed in a pure nitrogen atmosphere.[22] Other details of the experimental setup and signal analysis can be found elsewhere.[24,25]

In order to compare TA and THz data, we carried out TA test measurements in a nitrogen atmosphere using the excitation intensities utilized for THz experiment. We did not observe any change in the TA kinetics shape (see Supporting Information).

■ RESULTS AND DISCUSSION

Sample Characterization. The ZnO NWs grown for 4 h exhibit typical lengths ∼600 nm and diameters of 40−50 nm (Figure 1A). After sensitization, a layer with high roughness can be seen on the NWs surface by SEM (Figure 1B). HR-TEM images provide even more compelling evidence of the QDs anchoring onto the NWs surface. In Figure 1D, the CdSe QDs (visible (111) lattice planes) are clearly deposited on the NW surface (distinct (1010) lattice planes of ZnO).[26]

Absorption spectra of the CdSe QDs (Figure 2A, dashed lines) show a pronounced exciton band-edge component, typical for quantum-confined carriers. From the position of the band (514 to 551 nm) we estimated the mean size of the QDs in each sample.[11] The diameters (2.5 to 3.1 nm) are in good agreement with the HR-TEM results (Figure 1C-D).

After the deposition of QDs on ZnO NWs (Figure 2A, solid line), the absorbance spectrum becomes a sum of losses due to scattering by NWs (background signal) and absorption of the CdSe QDs (peak around 550 nm). The deposited QDs retain the band-like absorption structure, which is even more pronounced in the TA spectra described in the next section.

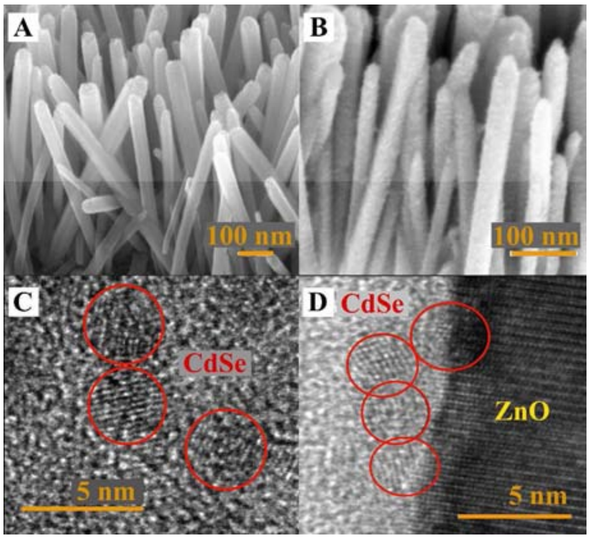

Figure 1. SEM images of (A) pristine ZnO NWs array, (B) ZnO NWs after 3.1 nm CdSe QDs sensitization for 2 h. (C) HR-TEM image of CdSe QDs. (D) HR-TEM image of CdSe QDs attached to a ZnO NW after sensitization; location of several QDs is outlined by circles as a visual aid.

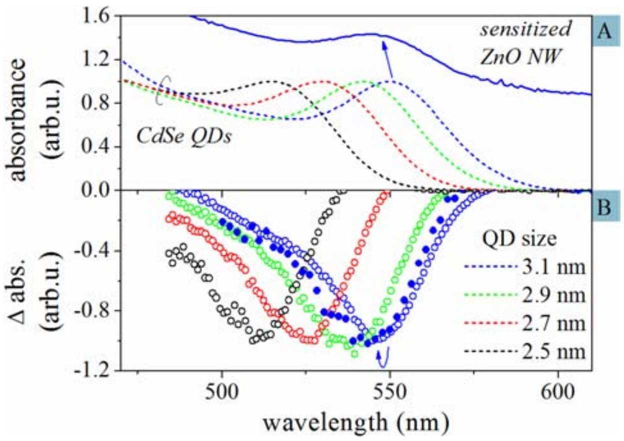

Figure 2. (A) Steady-state absorption spectra of CdSe QDs (dashed lines) compared to QD-sensitized ZnO NWs (solid line). (B) Transient absorption spectra of CdSe QDs (open circles) compared to QD-sensitized ZnO NWs (filled circles) − both cases for delay time 1 ps, $\lambda_{exc} = 470$ nm.

Transient Absorption. TA of both QD-sensitized ZnO NWs (Figure 2B, filled circles) and QDs (Figure 2B, open circles) shows an instantaneous bleach of the first exciton states. The bleach corresponds to state filling by electrons in QDs,[27] so that it can serve as a measure of the number of excited electrons per QD.

Although deposition of CdSe QDs on ZnO surface has very little effect on the shape of TA spectra, the TA kinetics changes drastically (see Figure 3).

We will first discuss the observed TA kinetics of unattached QDs. The multiexponential decay on a nanosecond time scale (A_1 = 10−20%, τ_1 = 0.5−2 ns; A_2 = 75−85%, τ_2 = 13 ns;) has the same character as previously reported decays of a single exciton in CdSe QDs affected by fluctuating rates of nonradiative processes (QDs charging, changes in surroundings in close proximity, etc.).[28,29] Besides the above two components, an initial minor drop in signal (5% of amplitude)

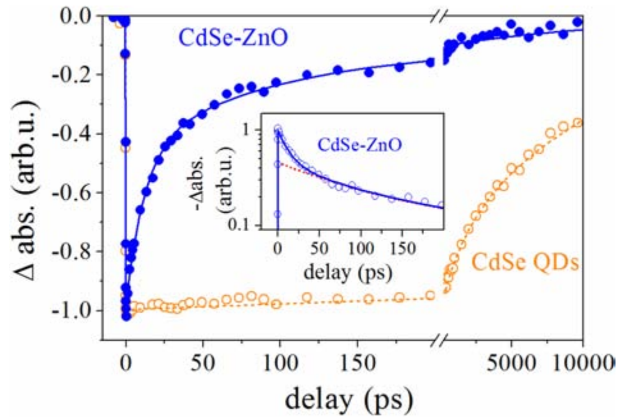

Figure 3. Transient absorption kinetics of CdSe QDs (orange open circles) and CdSe QDs attached to ZnO surface (blue filled circles); QDs follow a two-exponential fit (dashed line) before sensitization and a three-exponential fit (solid line) after sensitization; (Inset) Illustration of three-exponential fit (solid blue line) of QDs-sensitized ZnO TA kinetics (open circles), compared to sum of nanosecond component and slow component only (dotted red line); see text for the fitting details; QDs mean size is 3.1 nm, $\lambda_{\mathrm{exc}} = 470$ nm, $\lambda_{\mathrm{probe}} = 540$ nm.

during the first ~20 ps can be resolved, which corresponds to Auger recombination.[27] Since the observed TA dynamics of CdSe QDs are in good agreement with previous reports,[28,29] in the following we will focus on QDs deposited on ZnO NWs.

The TA signal decay appearing after NW sensitization by QDs has a three-exponential character (see Figure 3 inset, blue line). It consists of two dominant subnanosecond components followed by a minor nanosecond component. Throughout the text, we will refer to the components as 'fast component' (lifetimes 3−12 ps), 'slow component' (lifetimes 60−102 ps) and 'nanosecond component'. The nanosecond component can be well fitted by a single-exponential 13 ns decay observed previously for the pure QDs.

To avoid ambiguity concerning the origin of the fast dynamics, we deposited QDs on a SiO_2 surface, where no electron transfer can occur.[2] We verified that no shortening of TA kinetics of QDs appears (see Supporting Information).

The fast and slow components differ by almost an order of magnitude. However, a question may arise whether they correspond to separable components having different physical origin, or represent a broad distribution of transfer rates of the same transport process. We analyzed the kinetics by starting the curve-fitting optimization from a broad distribution of lifetimes. The best fit converged to two clearly distinguishable subdistributions with good correspondence to the above fast and slow components (see the Supporting Information for details).

Although a similar two-component subnanosecond decay has been widely observed for a number of QD−MO systems,[1−6] there is no consensus concerning assignment of the components. Depending on the particular case, either fast or slow decay is considered as an electron transfer from a QD to MO, whereas the other component is often attributed to different processes, such as electron surface trapping[1] or back-electron transfer in combination with carrier recombination.[2]

THz Spectroscopy. In order to distinguish underlying mechanisms of the TA decay, we carried out time-resolved THz spectroscopy measurements. The technique is sensitive to the number of excited electrons in ZnO and therefore can track their injection from CdSe QDs.

Spectral properties of photoinduced transient conductivity in QD-sensitized NWs are presented in Figure 4A, solid lines. The spectra are shown at three representative pump−probe delays and they are characterized by an increasing real part and decreasing imaginary part as a function of THz frequency. Such response is a signature of a transport of electrons moving freely within the MO NWs, similar to behavior observed in dye-sensitized ZnO nanoparticles.[24]

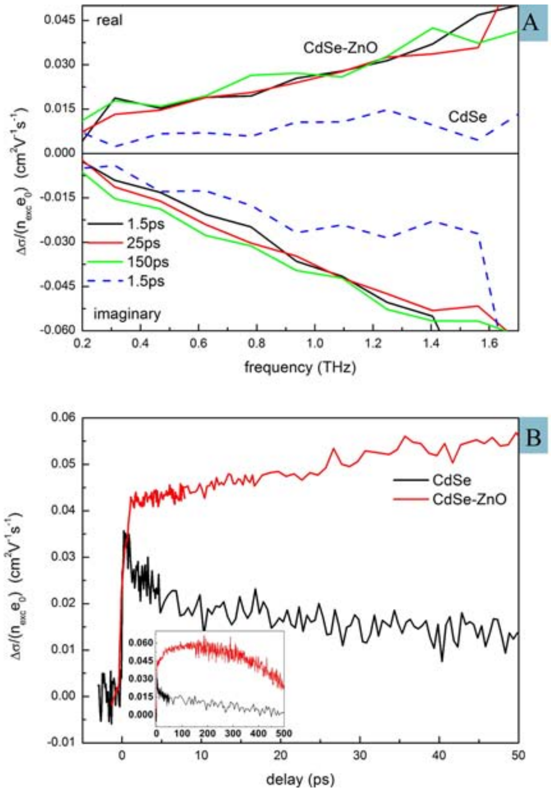

Figure 4. (A) Transient photoconductivity of QDs (dashed lines) and QD-sensitized NW (solid lines) normalized with excitation density at different pump probe delays. (B) Time evolution of transient photoconductivity.

The shape of the conductivity spectrum confirms that, already 1.5 ps after photoexcitation, electrons are injected from the QDs to the NWs. This might be partly a consequence of a fast electron injection from unthermalized electron states. However, time resolution of the THz measurements does not allow us to distinguish this injection pathway. For the two other representative delays, 25 and 150 ps after photoexcitation, we see very similar behavior.

For comparison, the THz spectrum of pure CdSe QDs is also presented in Figure 4A (dashed lines). It has a different shape. By using the same excitation conditions as for the QD-sensitized NW, we obtain the conductivity spectrum which has a small real part with no dependence on frequency while its imaginary part is similar with the QD-sensitized NW. The different behavior is caused by the electronic structure of QDs. Since the THz-radiation photon (probe) energy is too small to induce any transitions in the conduction band, the THz signal is more affected by holes in the valence band. In such cases the expected THz dielectric function is mostly real i.e. negligible real conductivity and finite imaginary conductivity, as it was reported by Beard et al. for CdSe QDs.[30]

Different shapes of the THz spectra for pure QDs and QD-sensitized NWs further confirm our assertion that charge transfer occurs. If it were not so, one would expect the same shape of THz spectra in both cases.

In Figure 4B we present the time-dependent change in the THz signal (photoinduced transient conductivity) for QDs only (black line) and QD-sensitized NWs (red line). At zero time, the kinetic curves show an instrument response limited instantaneous rise due to photoexcitation of the QDs. The amplitudes of the instantaneous change in the photoconductivity, normalized to excitation density $\Delta\sigma/(n_{\mathrm{exc}}e_0)$ differ about 20% for the two samples.

The difference in the instantaneous signal amplitude can stem from multiple origins. THz signal amplitude is proportional to a product of concentration of charge carriers and their mobility. In the two samples, the concentration normalized to the excitation intensity is the same. However, part of the excited electrons in QDs might be injected into ZnO via the so-called hot electron transfer, hence increasing the instantaneous THz signal. Another possible mechanism is a change in electron mobility in QD due to attachment to ZnO.

In the pure QDs the initial rise is followed by a rapid decay component due to Auger recombination. The average excitation density $N = 1.2$ is expected to cause a decay by approximately 35% with lifetime of about 15 ps[27] followed by a long-lived signal in good agreement with the observed kinetics.

The THz kinetics of QD-sensitized NWs is very different. The instantaneous rise is followed by an additional fast and clearly distinguishable rising component during the first few picoseconds. Apparently, the QDs cannot be responsible for this additional rise in THz signal. We will show later that this is due to the appearance of electrons with high mobility in ZnO. After the initial phase a slower increase in the time-scale of 100 ps occurs (see inset of Figure 4B). At longer time scale the THz signal decays, which we attribute to electron trapping in ZnO.[24]

Fast Component: Electron Injection. To summarize the results, the TA kinetics features the fast decay component ($\tau \approx$ 10 ps), signaling a decreasing number of excited electrons in QDs; meanwhile, the THz spectroscopy kinetics gives a rising signal occurring on the same time scale, showing an increase in the population of mobile electrons.

The only feasible explanation for our observations is that there is an ultrafast transfer of electrons from QDs to ZnO. Any other process, such as electron surface trapping, electron relaxation, or electron−hole recombination, would only lead to a decay of the THz signal.[30,31]

Such ultrafast transfer has important implications for exploiting the multiple exciton generation in QD-sensitized solar cells. In this context the injection has to occur faster than competing loss channels, e.g. Auger recombination of the excited electrons. The measured injection time scale here is indeed faster than the corresponding Auger recombination.[27]

Previously, electron transfer has often been implicated indirectly on the basis of agreements between transfer rates and Marcus theory. We used the same approach in our case and carried out TA measurements for different mean QD sizes (see Figure 5, left panels).

Since the TA lifetime of pure QDs is considerably longer than the TA decay of the CdSe−ZnO system, we can use the fast and slow components directly in analyses of the corresponding rate processes without correcting for the QDs' lifetime.

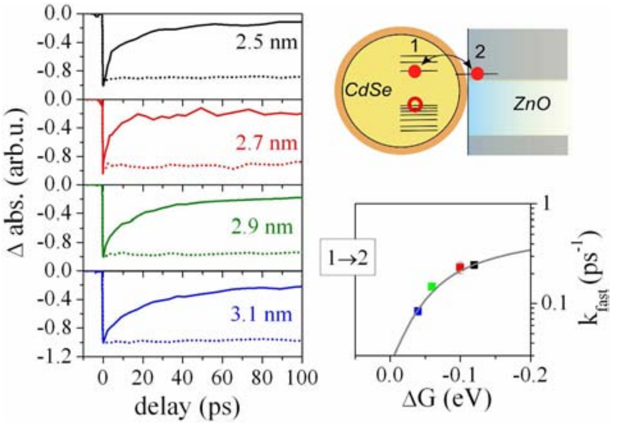

Figure 5. (Left) Normalized TA kinetics of pure QDs (dotted lines) and sensitized ZnO NWs (solid lines) with different QD sizes (measured in spectral position of sample maximum signal). (Top right) Scheme of reversible initial electron transfer from QD (1) to NW (2). (Bottom right) Dependence of fast TA decay rate (solid squares) described by Marcus theory (gray line) (see text for details), λ_{exc} = 470 nm; λ_{probe} (2.5 nm) = 506 nm, λ_{probe} (2.7 nm) = 516 nm, λ_{probe} (2.9 nm) = 526 nm, λ_{probe} (3.1 nm) = 540 nm.

According to the Marcus theory of electron transfer,[32] the rate depends on free energy change ΔG. The latter is a sum of electron energy difference ΔE_{el} in the QD and the MO conduction bands, and the Coulombic energy change ΔE_{C} arising from interaction between electron and hole.

Alignment of energy states in CdSe−ZnO system has been measured experimentally by Carlson et al.[33] For our samples the ΔE_{el} reaches values between −0.7 to −0.95 eV, depending on QD size (see Supporting Information for details). The electron energy difference acts as a driving force for the electron transfer.

On the contrary, the Coulombic interaction acts against electron transfer. It increases ΔG value, because the final state (electron in ZnO and hole in QD) has higher Coulombic energy compared to the initial state (both electron and hole in QD). The difference can be calculated by employing the theory of Tvrdy et al.,[2] where the electron charge is assumed to stay on the ZnO surface:

$$\Delta E_{\mathrm{C}} = \frac{1.786 e^2}{\varepsilon_{\mathrm{QD}} R_{\mathrm{QD}}} + \frac{e^2}{2 R_{\mathrm{QD}}}\left(1 + \frac{0.786}{\varepsilon_{\mathrm{QD}}}\right) - \frac{e^2}{4(R_{\mathrm{QD}} + h)}\frac{\varepsilon_{\mathrm{MO}} - 1}{\varepsilon_{\mathrm{MO}} + 1} \quad (1)$$

For the previously reported values of QD permittivity ($\varepsilon_{\mathrm{QD}}$ = 6.1),[2] MO permittivity ($\varepsilon_{\mathrm{MO}}$ = 10.5),[2] known radii of QDs R_{QD}, and QD−MO distance h (linker layer thickness of 0.65 nm),[34] eq 1 leads to values ranging from 0.66 to 0.83 eV. As one can see, the interaction between electron and hole has a substantial effect on ΔG and for our system it has the same scale as the electron energy level difference.

Knowledge of the ΔG value allows us to calculate resulting electron transfer rate dependence. In our case the electron is transferred from a discrete electron state in the QD to a continuum of states in the MO, that is weighted by the density of states $\rho(E) \propto (E - E_g)^{1/2}$. This leads to the following expression for the rate constant (see Supporting Information for more details):[2]

$$k_t = C \int \sqrt{E - E_g} \exp\left(-\frac{(\lambda + \Delta G + E)^2}{4\lambda kT} \right) dE \qquad (2)$$

The scaling factor C includes all energy-independent coefficients of eq 2 (density of states prefactors, Marcus theory prefactors, etc.) including the QD−MO wave function overlap. This overlap is assumed not to change with the QD size. In our case this approximation can be applied, because the curve shape is dominated by changes in ΔG values, whereas the change in QD size is small. If this were not so, it would also be essential to account also for the change in the wave functions overlap, as shown by E. Canovas et al.[35,36]

By adopting previous estimates of the system reorganization energy λ (30 meV for CdSe QDs covered by alkanethiols),[7] we obtain a theoretical model represented by eq 2, which has only one fitting parameter, C. Figure 5 (bottom right panel) demonstrates that the fast component decay rates can be well fitted by the Marcus theory.

Slow Component: Slower Injection or Dynamics in ZnO? Besides the fast component, our experiments also show a slow component with typical lifetime of about 80 ps in both TA and THz kinetics. Signals on this time scale correspond to a decay of TA signal and simultaneous THz signal rise (see Figure 4B, inset).

The most straightforward explanation of the observed two-component kinetics is heterogeneous electron injection (HI) into ZnO (see Figure 6B). In other words, we might observe electron injection from two classes of QDs with two rates of electron transfer. From the ratio of the fast and slow component amplitudes in TA measurements, we can estimate that the 'slowly injecting' QDs ($\tau \approx 60-100$ ps) should account for about 30−50% of all QDs.

This slow injection rate might result from QD agglomeration—electrons are either injected directly from more distant QDs or via another QD.[37−39] Although our samples do contain agglomerated QDs (see Figure 1D), according to the analysis of the TEM images, the agglomeration accounts for less than 10% of the QDs and cannot be responsible for a ~40% slow component contribution in the TA kinetics (see Figure 3 Inset).

Different QD anchoring to MO might also affect electron transfer. However, by comparing size of the QD (about 3 nm) and the linker layer thickness (about 0.5 nm), it is obvious that several linker molecules contribute to the QD−MO anchoring. In such a case, different molecules' conformations would lead to a single broad distribution of lifetimes, rather than two distinct components.

Finally, the HI can also be caused by electron trapping and consequent transport into ZnO. This effect has been reported before for SILAR-prepared CdSe−ZnO system.[37] However, in this case the initial kinetics in the THz signal (corresponding to the fast component in TA kinetics) should show a complex behavior, where the THz signal is partly decreasing due to the electron trapping and partly increasing due to the fast electron transfer. No such feature in the THz kinetics was observed for our samples

An alternative explanation of the two-component kinetics is a two-step electron transfer via a CTS (see Figure 6A). The CTS formation has been observed previously by several groups for dye−ZnO systems.[24,40,41] Also the CTS dissociation time of 200 ps reported by Nemec et al. for dye−ZnO system agrees well with our THz dynamics.[24]

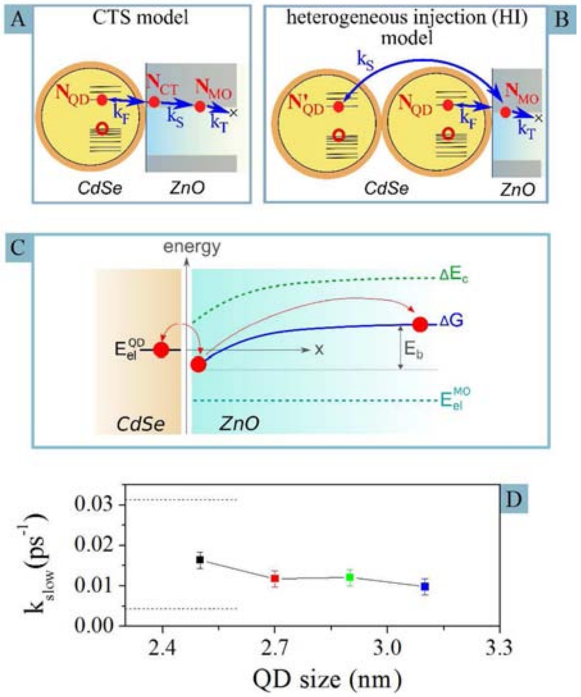

Figure 6. (A, B) Schemes of electron injection via charge transfer state (CTS) and heterogeneous injection (HI). (C) Scheme of free energy change in system ΔG (solid blue line) as an interplay between difference in electron states energies ΔE_{el} (dashed cyan line) and Coulombic interaction ΔE_C (dashed green line) leading to CTS formation. (D) Rate of slow component of TA kinetics for QDs with different sizes (solid squares) compared to range of theoretically predicted dissociation rates of CTS from eq 3 (dashed lines) (see text for details).

In case of the CTS scenario, there is a fast electron transfer at the early time scale (see Figure 6C). However, the THz signal does not reach its maximum until 200 ps, because the injected electrons initially have a reduced mobility due to the CTS formation. Continuous dissociation of the CTS increases the photoconductivity until 200 ps where most if not all of the electrons are released to the bulk of ZnO NWs.

Electron transfer from QD to MO (forward transfer) is always accompanied by a back-transfer of electrons from MO to QD (see schemes in Figures 4 and 6). This holds for every donor−acceptor system leading to a thermodynamic equilibrium. Therefore, the CTS dissociation can be observed also in the TA signal, which reflects the population of electrons in QDs. Quantitative calculation of the back-transfer effect on TA kinetics is in good agreement with our measurements (see Supporting Information).

We can gain insight into the possibility of CTS formation from a balance of free energy difference ΔG due to an electron injection to MO ($\Delta G = \Delta E_{el} + \Delta E_C$; see Figure 6C). Previously, we assumed that the electrons are transferred from QDs to the MO, where they stay bound to holes due to the Coulombic interaction (see eq 1).

If electrons were rather injected into the volume of ZnO NW, the electron−hole Coulombic interaction would be negligible. This can be represented by $h \to \infty$ in eq 1. In this case, the ΔE_C values are increased by 140−160 meV and the total ΔG values become positive (see Figure 6C). This implies that the direct electron injection into the ZnO bulk is very unlikely and suggests that electrons might tend to stay localized in the intermediate CTS.

We point out that the described localization does not correspond to an electron trapping on ZnO surface defects. For the Coulombic interaction featuring a weak spatial dependence ($1/r$), a localized electron wave function will still be spread over a number of atoms in the MO.

There are several possible mechanisms of CTS dissociation, namely electron−phonon or electron−electron interaction, solvent reorganization, electron relaxation to lower bulk states, or electron back-recombination with the hole. Because all processes can be acting in parallel, it is practically impossible to predict the exact CTS lifetime. Yet, we can get an idea about the expected CTS dissociation rate k_{diss} from the electron−phonon interaction determined by the Braun−Onsager model:[42]

$$k_{\mathrm{diss}} = \frac{\mu e}{\varepsilon_0 \varepsilon_{\mathrm{QD}}} \frac{3}{4\pi a^3} \exp\left(-\frac{E_{\mathrm{b}}}{kT}\right) \tag{3}$$

Electron mobility μ for ZnO NWs prepared by the hydrothermal synthesis has been reported to be 1−5 $\mathrm{cm^2\ V^{-1}\ s^{-1}}$.[43] Coulombic binding energy of CTS E_{b} has been calculated from eq 1 as additional energy needed to overcome the electron−hole Coulombic interaction (140−160 meV). Finally, thermalization radius a can be expressed as $a = e^2/(4\varepsilon_0\varepsilon_{\mathrm{MO}}E_{\mathrm{b}})$. The resulting rough estimate of the CTS dissociation time of 40−200 ps (see Figure 6D, dashed lines) corresponds well to the time scale of the slow component observed in the TA measurements (60−100 ps, see Figure 6D, solid squares) and the slow rise in the THz measurements.

TA and THz Comparison. Changes in the TA and THz signal during the first 150 ps after excitation are shown in Figure 7A. Note that, in order to provide a better comparison of the dynamics, the instantaneous rise of the THz signal is truncated in Figure 7. TA kinetics is governed by the fast two-exponential decay, as we have described before ($\tau_{\mathrm{F}} = 12$ ps, $\tau_{\mathrm{S}} = 100$ ps), and we will demonstrate that the same rates determine the THz kinetics.

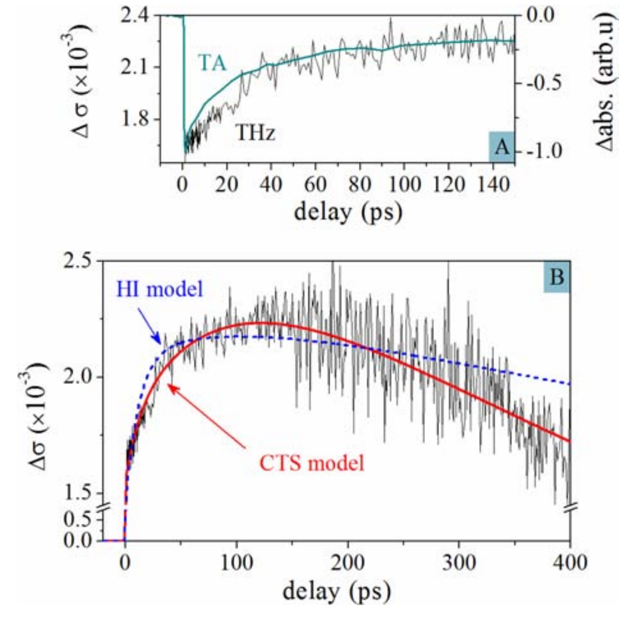

Figure 7. (A) Normalized TA kinetics (cyan line) compared to THz kinetics (black line). (B) Measured THz kinetics (black line) compared to CTS (solid red line) and HI (dashed blue line) model calculations. QDs mean size 3.1 nm; TA $\lambda_{\mathrm{probe}} = 540$ nm.

In case of the HI, two components of TA decay reflect a continuously decreasing number of electrons in QDs, and the transferred electrons increase accordingly with the THz signal. Therefore, the TA decay is expected to have the same shape as the THz signal rise. However, the normalized TA and THz kinetics in Figure 7A clearly differ in their shapes. We conclude that the HI does not describe simultaneously the measured TA and THz data.

In the following we carry out quantitative comparison of the TA and THz data on the basis of the kinetic equations describing the two proposed models (HI and CTS models). First, we investigate the possibility of the CTS formation by employing the model depicted in Figure 6A. We use the following rate equations to calculate the number of electrons in QD (N_{QD}), CTS (N_{CT}), and MO (N_{MO}):

$$\frac{\mathrm{d}N_{\mathrm{QD}}(t)}{\mathrm{d}t} = +g(t) - k_{\mathrm{F}}N_{\mathrm{QD}}(t) \tag{4}$$

$$\frac{\mathrm{d}N_{\mathrm{CT}}(t)}{\mathrm{d}t} = +k_{\mathrm{F}}N_{\mathrm{QD}}(t) - k_{\mathrm{S}}N_{\mathrm{CT}}(t) \tag{5}$$

$$\frac{\mathrm{d}N_{\mathrm{MO}}(t)}{\mathrm{d}t} = +k_{\mathrm{S}}N_{\mathrm{CT}}(t) - k_{\mathrm{T}}N_{\mathrm{MO}}(t) \tag{6}$$

The electrons are excited in QDs by a generating function $g(t) = \delta(t)$. In order to account for the later-stage THz decay, a process of electron trapping in MO (rate k_{T}) was included.

The resulting THz signal can be calculated as:

$$\Delta\sigma = N_{\mathrm{QD}}\Delta\sigma_{\mathrm{QD}} + N_{\mathrm{CT}}\Delta\sigma_{\mathrm{CT}} + N_{\mathrm{MO}}\Delta\sigma_{\mathrm{MO}} + N_{\mathrm{H}}\Delta\sigma_{\mathrm{H}} \tag{7}$$

where $\Delta\sigma_{\mathrm{QD/CT/MO}}$ stands for the THz signal of electron at each state. The holes' contribution to the THz signal is included by $\Delta\sigma_{\mathrm{H}}$ (THz signal of hole) and N_{H} denotes the number of holes. As the holes are located in QDs for the whole studied period, we assume that their number is not changing and the corresponding THz signal stays constant. Detailed description of the model can be found in the Supporting Information.

The rates used in the calculation are set from TA measurements ($k_{\mathrm{F}} = {}^{1}/_{12}\ \mathrm{ps^{-1}}$, $k_{\mathrm{S}} = {}^{1}/_{100}\ \mathrm{ps^{-1}}$); the values of $\Delta\sigma$, together with MO trapping rate k_{T} are left as fitting parameters. As shown in Figure 7B (solid red line) the CTS model can well describe the THz kinetics ($\Delta\sigma_{\mathrm{CT}} = 1.35\Delta\sigma_{\mathrm{QD}}$;$\Delta\sigma_{\mathrm{MO}} = 2.1\Delta\sigma_{\mathrm{QD}}$; see the Supporting Information for details). Hence, the TA and THz kinetics can be described simultaneously by the CTS model.

The presented model predicts for the delays after 400 ps a slower THz signal decay than the one observed. We attribute it to a possible electron−hole recombination or to some processes in MO, which are not included in our model.

At the same time we tested the HI model (see Figure 6B) using the rate equation approach. In this case we have two types of QDs (N_{QD},N'_{QD}), leading to the following rate equations:

$$\frac{\mathrm{d}N_{\mathrm{QD}}(t)}{\mathrm{d}t} = +0.7g(t) - k_{\mathrm{F}}N_{\mathrm{QD}}(t) \tag{8}$$

$$\frac{dN'_{QD}(t)}{dt} = +0.3g(t) - k_S N'_{QD}(t) \tag{9}$$

$$\frac{dN_{MO}(t)}{dt} = +k_F N_{QD}(t) + k_S N'_{QD}(t) - k_T N_{MO}(t) \tag{10}$$

The generating term $g(t) = \delta(t)$ is divided between the two QDs groups according to the fast and slow component proportions in TA kinetics (see Supporting Information for detailed information). We assume that both types of QDs feature the same THz signal:

$$\Delta\sigma = (N_{QD} + N'_{QD})\Delta\sigma_{QD} + N_{MO}\Delta\sigma_{MO} + N_H\Delta\sigma_H \tag{11}$$

The THz kinetics calculated from this model does not agree with the measured signal shape for any set of parameters. The best fit (see Figure 7B, dashed blue line) was obtained for $\Delta\sigma_{MO} = 1.7\Delta\sigma_{QD}$ (see Supporting Information for details).

We conclude that the comparison between TA and THz data strongly supports the possibility of the CTS-mediated electron injection rather than the HI scenario.

The formation of CTS would have important implications for the studies of dynamics in QD-sensitized SCs. To date, the electron transfer rate from QDs to MO has been considered as the most important parameter. Nevertheless, properties of MO (in particular the MO permittivity and electron mobility), which affect CTS formation and dissociation might, in fact, be the crucial factors for the resulting conversion efficiency. This effect may be a part of the observed inconsistencies between the electron transfer rates and the SCs efficiencies.[2]

■ CONCLUSIONS

We present experimental results which directly prove that electrons are injected from QDs to MO already on a picosecond time scale (fast component of TA decay and corresponding rise in THz signal). This means that the electron transport takes place considerably faster than the Auger recombination, pointing out the multiple electron collection as a feasible scenario for QD-sensitized solar cells.

Furthermore, we observe two-component kinetics for both TA and THz data, which can be a result of heterogeneous electron injection to ZnO, or a sign of electron injection via a CTS. Our results strongly support the scenario of CTS-mediated injection.

■ ASSOCIATED CONTENT

Ⓢ Supporting Information

Details of sample preparation, characterization, data fitting, Marcus theory and electron back-transfer calculations, and rate equation models. This material is available free of charge via the Internet at http://pubs.acs.org.

■ AUTHOR INFORMATION

Corresponding Author

Tonu.Pullerits@chemphys.lu.se

Author Contributions

‡These authors contributed equally.

Notes

The authors declare no competing financial interest.

■ ACKNOWLEDGMENTS

We gratefully acknowledge financial support of the Swedish Research Council, the Knut and Alice Wallenberg Foundation, Crafoord foundation, Swedish Energy Agency, and the Swedish Foundation for Strategic Research. We thank Nils Lenngren and Torbjörn Pascher for their help with time-resolved experiments, and Wilfred Fullagar for valuable comments. Collaboration within nmC@LU is acknowledged.

■ REFERENCES

(1) Pernik, D. R.; Tvrdy, K.; Radich, J.; Kamat, P. V. *J. Phys. Chem. C* **2011**, *115*, 13511.

(2) Tvrdy, K.; Frantsuzov, P. A.; Kamat, P. V. *Proc. Natl. Acad. Sci. U.S.A.* **2011**, *108*, 29.

(3) Blackburn, J. L.; Selmarten, D. C.; Nozik, A. J. *J. Phys. Chem. B* **2003**, *107*, 14154.

(4) Robel, I.; Subramanian, V.; Kuno, M.; Kamat, P. V. *J. Am. Chem. Soc.* **2006**, *128*, 2385.

(5) Robel, I.; Kuno, M.; Kamat, P. V. *J. Am. Chem. Soc.* **2007**, *129*, 4136.

(6) Guijarro, N.; Shen, Q.; Giménez, S.; Mora-Seró, I.; Bisquert, J.; Lana-Villarreal, T.; Toyoda, T.; Gómez, R. *J. Phys. Chem. C* **2010**, *114*, 22352.

(7) Tisdale, W. A.; Zhu, X.-Y. *Proc. Natl. Acad. Sci. U.S.A* **2011**, *108*, 965.

(8) Shalom, M.; Dor, S.; Ruhle, S.; Grinis, L. *J. Phys. Chem. C* **2009**, *2*, 3895.

(9) Sambur, J. B.; Novet, T.; Parkinson, B. A. *Science* **2010**, *330*, 63.

(10) Guijarro, N.; Lana-Villarreal, T.; Mora-Seró, I.; Bisquert, J.; Gómez, R. *J. Phys. Chem. C* **2009**, *113*, 4208.

(11) Yu, W. W.; Qu, L.; Guo, W. *Chem. Mater.* **2003**, *15*, 2854.

(12) Zhang, Q.; Guo, X.; Huang, X.; Huang, S.; Li, D.; Luo, Y.; Shen, Q.; Toyoda, T.; Meng, Q. *Phys. Chem. Chem. Phys.* **2011**, *13*, 4659.

(13) Rühle, S.; Shalom, M.; Zaban, A. *ChemPhysChem* **2010**, *11*, 2290.

(14) Dibbell, R. S.; Watson, D. F. *J. Phys. Chem. C* **2009**, *113*, 3139.

(15) Pijpers, J.; Koole, R.; Evers, W.; Houtepen, A.; Boehme, S.; de Mello Donegá, C.; Vanmaekelbergh, D.; Bonn, M. *J. Phys. Chem. C* **2010**, 18866.

(16) Greene, L. E.; Yuhas, B. D.; Law, M.; Zitoun, D.; Yang, P. *Inorg. Chem.* **2006**, *45*, 7535.

(17) Sudhagar, P.; Chandramohan, S.; Kumar, R. S.; Sathyamoorthy, R.; Hong, C.-H.; Kang, Y. S. *Phys. Status Solidi A* **2011**, *208*, 474.

(18) Sun, X. W.; Chen, J.; Song, J. L.; Zhao, D. W.; Deng, W. Q.; Lei, W. *Opt. Express* **2010**, *18*, 1296.

(19) Kharkwal, A.; Sharma, S. N.; Chand, S.; Singh, a. K. *Colloid Polym. Sci.* **2011**, *290*, 49.

(20) Barceló, I.; Lana-Villarreal, T.; Gómez, R. *J. Photochem. Photobiol. A* **2011**, *220*, 47.

(21) Leschkies, K. S.; Divakar, R.; Basu, J.; Enache-Pommer, E.; Boercker, J. E.; Carter, C. B.; Kortshagen, U. R.; Norris, D. J.; Aydil, E. S. *Nano Lett.* **2007**, *7*, 1793.

(22) Tvrdy, K.; Kamat, P. V. *J. Phys. Chem. A* **2009**, *113*, 3765.

(23) Žídek, K.; Zheng, K.; Chábera, P.; Abdellah, M.; Pullerits, T. *Appl. Phys. Lett.* **2012**, *100*, 243111.

(24) Němec, H.; Rochford, J.; Taratula, O.; Galoppini, E.; Kužel, P.; Polívka, T.; Yartsev, A.; Sundström, V. *Phys. Rev. Lett.* **2010**, *104*, 1.

(25) Ulbricht, R.; Hendry, E.; Shan, J.; Heinz, T.; Bonn, M. *Rev. Mod. Phys.* **2011**, *83*, 543.

(26) Leschkies, K. S.; Beatty, T. J.; Kang, M. S.; Norris, D. J.; Aydil, E. S. *ACS Nano* **2009**, *3*, 3638.

(27) Klimov, V. I. *Annu. Rev. Phys. Chem.* **2007**, *58*, 635.

(28) Schlegel, G.; Bohnenberger, J.; Potapova, I.; Mews, A. *Phys. Rev. Lett.* **2002**, *88*, 137401.

(29) Sharma, S. N.; Pillai, Z. S.; Kamat, P. V. *J. Phys. Chem. B* **2003**, *107*, 10088.

(30) Beard, M. C.; Turner, G. M.; Schmuttenmaer, C. A. *Nano Lett.* **2002**, *2*, 983.

(31) Mics, Z.; Němec, H.; Rychetský, I.; Kužel, P.; Formánek, P.; Malý, P.; Němec, P. *Phys. Rev. B* **2011**, *83*, 1.

(32) Marcus, R. A. *J. Chem. Phys.* **1956**, *24*, 966.

(33) Carlson, B.; Leschkies, K.; Aydil, E. S.; Zhu, X.-Y. *J. Phys. Chem. C* **2008**, *112*, 8419.

(34) Bain, C. D.; Troughton, E. B.; Tao, Y. T.; Evall, J.; Whitesides, G. M.; Nuzzo, R. G. *J. Am. Chem. Soc.* **1989**, *111*, 321.

(35) Cánovas, E.; Moll, P.; Jensen, S.; Gao, Y.; Houtepen, A. J.; Siebbeles, L. D.; Kinge, S.; Bonn, M. *Nano Lett.* **2011**, *11*, 5234.

(36) Koole, R.; Liljeroth, P.; de Mello Donegá, C.; Vanmaekelbergh, D.; Meijerink, A. *J. Am. Chem. Soc.* **2006**, *128*, 10436.

(37) Guijarro, N.; Lana-Villarreal, T.; Shen, Q.; Toyoda, T.; Gómez, R. *J. Phys. Chem. C* **2010**, 21928.

(38) Hodes, G. *J. Phys. Chem. C* **2008**, *112*, 17778.

(39) Kagan, C. R.; Murray, C. B.; Nirmal, M.; Bawendi, M. G. *Phys. Rev. Lett.* **1996**, *76*, 1517.

(40) Furube, A.; Katoh, R.; Yoshihara, T.; Hara, K.; Murata, S.; Arakawa, H.; Tachiya, M. *J. Phys. Chem. B* **2004**, *108*, 12583.

(41) Stockwell, D.; Yang, Y.; Huang, J.; Anfuso, C.; Huang, Z.; Lian, T. *J. Phys. Chem. C* **2010**, *114*, 6560.

(42) Deibel, C.; Strobel, T.; Dyakonov, V. *Adv. Mater.* **2010**, *22*, 4097.

(43) Law, M.; Greene, L. E.; Johnson, J. C.; Saykally, R.; Yang, P. *Nat. Mater.* **2005**, *4*, 455.